

Supplement of Atmos. Chem. Phys., 17, 13491–13508, 2017
<https://doi.org/10.5194/acp-17-13491-2017-supplement>
© Author(s) 2017. This work is distributed under
the Creative Commons Attribution 3.0 License.



Supplement of

Secondary organic aerosol from chlorine-initiated oxidation of isoprene

Dongyu S. Wang and Lea Hildebrandt Ruiz

Correspondence to: Lea Hildebrandt Ruiz (lhr@che.utexas.edu)

The copyright of individual parts of the supplement might differ from the CC BY 3.0 License.

S1 Derivation of ΔVOC_{\min}

An expression for ΔVOC_{\min} , the minimum amount of VOC reacted required for SOA formation, can be obtained by rearranging Eq. (7) and (8) from the main text, which are parts of the volatility basis set (VBS) framework (Donahue et al., 2006),

$$5 \quad \frac{1}{\Delta VOC} = \frac{\sum_i \alpha_i \xi_i}{C_{OA}} \quad (S1)$$

$$\frac{1}{\Delta VOC} = \frac{\sum_i \alpha_i \left(1 + \frac{C_i^*}{C_{OA}}\right)^{-1}}{C_{OA}} \quad (S2)$$

$$\frac{1}{\Delta VOC} = \frac{C_{OA}}{C_{OA}} \sum_i \frac{\alpha_i}{C_i^* + C_{OA}} \quad (S3)$$

$$\frac{1}{\Delta VOC} = \sum_i \frac{\alpha_i}{C_i^* + C_{OA}} \quad (S4)$$

$$\frac{1}{\Delta VOC_{\min}} = \sum_i \frac{\alpha_i}{C_i^*} \quad (C_{OA} = 0) \quad (S5)$$

10 Equation (S5) can also be obtained via L'Hôpital's rule, starting from Eq. (S3)

$$\lim_{C_{OA} \rightarrow 0} \frac{1}{\Delta VOC} = \lim_{C_{OA} \rightarrow 0} \frac{C_{OA}}{C_{OA}} \left[\frac{\alpha_1}{C_1^* + C_{OA}} \dots \frac{\alpha_n}{C_n^* + C_{OA}} \right] \quad (S6)$$

$$\lim_{C_{OA} \rightarrow 0} \frac{1}{\Delta VOC} = \lim_{C_{OA} \rightarrow 0} \frac{\frac{d}{dC_{OA}} [C_{OA} \sum_i \left(\frac{\alpha_i}{C_i^*} \prod_j C_j^* \right) + C_{OA}^0(\dots) + C_{OA}^{M \geq 2}(\dots)]}{\frac{d}{dC_{OA}} [C_{OA} \prod_j C_j^* + C_{OA}^0(\dots) + C_{OA}^{M \geq 2}(\dots)]} \quad (S7)$$

15 Where the terms involving C_{OA}^0 become 0 and the terms involving $C_{OA}^{M \geq 2}$ are much smaller than terms involving $C_{OA}^{M \leq 1}$, and could therefore be neglected.

$$\lim_{C_{OA} \rightarrow 0} \frac{1}{\Delta VOC} = \lim_{C_{OA} \rightarrow 0} \left[\frac{\prod_j C_j^* \sum_i \frac{\alpha_i}{C_i^*}}{\prod_j C_j^*} \right] \quad (S8)$$

$$20 \quad \frac{1}{\Delta VOC_{\min}} = \sum_i \frac{\alpha_i}{C_i^*} \quad (S5)$$

Equation (S5) is the same as Eq. (9) in the main text.

S2 SOA oxidation state parameterization

From f_{44} , O:C, H:C, and \overline{OS}_C can be estimated as described in the literature (Canagaratna et al., 2015; Donahue et al., 2012; Heald et al., 2010; Kroll et al., 2011)

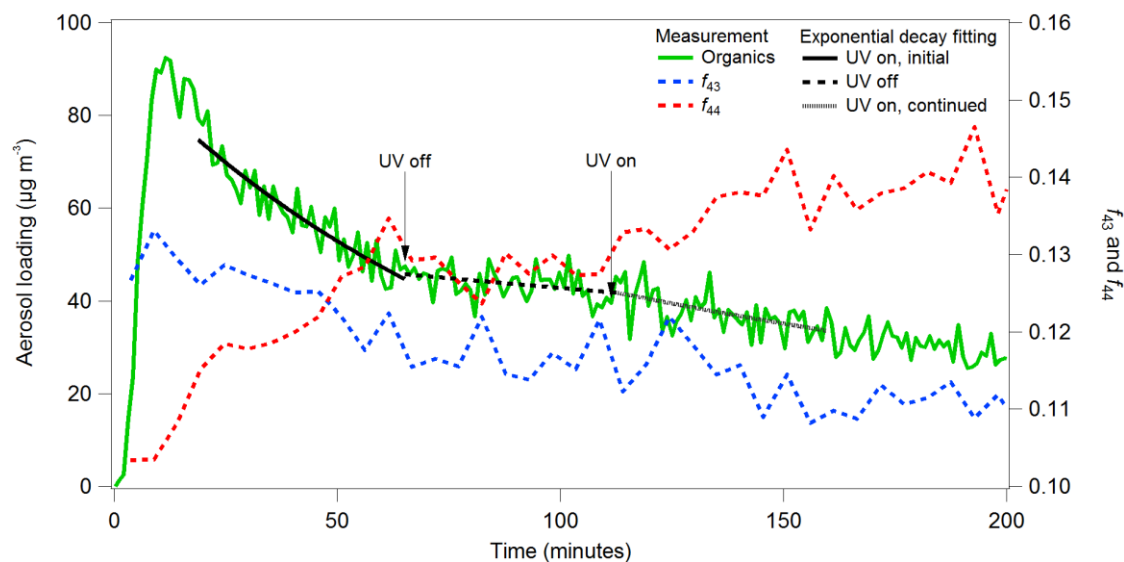
$$O:C = 0.079 + 4.31 \times f_{44} , \quad (S9)$$

$$5 \quad H:C = 2 - O:C , \quad (S10)$$

$$\overline{OS}_C \cong 3 \times O:C - 2 , \quad (S11)$$

$$\overline{OS}_C \cong 12.93 \times f_{44} - 1.842 , \quad (S12)$$

Deviation from Eq. (S11) could occur due to the presence of peroxide or heteroatom groups (Kroll et al., 2011), such as chloroalkyl hydroperoxide compounds identified in CISM measurements in this study. UV lights were turned off early during
 10 Exp. A5. As shown in Fig S1, the SOA extent of oxidation (f_{44} and f_{43}) was stable in the absence of UV, indicating that dark reactions, if present, did not affect the SOA extent of oxidation. Some wall-loss-corrected SOA concentration decrease was observed in the dark, possibly due to loss of organic vapor to the clean chamber wall and/or higher depositional loss rates of organics compared to sulfate due to a size-dependent org/sulfate ratio (Hildebrandt et al., 2009). The wall loss effects were smaller than aerosol aging effects, as shown in Fig. S1. Exponential decay functions were fitted to the depositional wall-loss
 15 corrected SOA concentrations during the initial rapid decay period, the dark period when UV lights were turned off, and during the continued oxidation period when UV lights were turned back on. The exponent of decay were, in chronological order, $1.1 \times 10^{-2} \text{ min}^{-1}$, $2.1 \times 10^{-3} \text{ min}^{-1}$, and $5.0 \times 10^{-3} \text{ min}^{-1}$.



20 **Figure S1:** Depositional wall loss-corrected SOA concentration and five-minute averages of f_{44} , and f_{43} observed for Exp A5. UV lights were turned on and off as labeled. f_{44} and f_{43} could be interpreted as proxies for oxidized and fresh SOA components, respectively, which did not evolve in the dark. SOA loss was observed in the dark, possibly due to loss of organic vapor to the Teflon® wall surfaces or differences in the depositional loss rates of organic and sulfate aerosol. Exponential fitting was applied to three separate 60-minute SOA concentration data segments during the initial photooxidation period, UV off period, and continued photooxidation period.

S3 CIMS signal normalization: ACIMS vs P-ACIMS

Chemical ionization by hydronium-water ion clusters in the CIMS could be described as



where X (“M” in the main text) represents an analyte and $H_3O^+(H_2O)_n$ represents the hydronium-water reagent cluster. k is the protonation rate coefficient (de Gouw and Warneke, 2007; Sellegri et al., 2005). A reverse of the above process is possible, but could be minimized via instrument tuning (Sellegri et al., 2005). For a compound with known proton affinity, the number of water clusters involved in the protonation process, n , is known as well. The proton affinity of isoprene is higher than that of H_3O^+ and lower than that of $(H_3O)^+H_2O$, meaning that n is 0 for isoprene, which could only extract the hydrogen from H_3O^+ , forming $C_5H_9^+$, which was observed in our measurements. The charge transfer product ion, $C_5H_8^+$ was also observed. In addition, $C_5H_7^+$, likely a hydride abstraction product by minor reagent ions such as NO^+ or O_2^+ , was also observed. However, fragmentation of oxidized products by $H_3O^+(H_2O)_n$ or minor O_2^+ ions could also produce $C_5H_7^+$ ion fragments.

Instrument sensitivity may change over the course of an experiment or between experiments and needs to be accounted for. For simplification, consider a single analyte and hydronium reagent ion. The active Chemical Ionization Mass Spectroscopy (ACIMS) formula could be applied to account for the sensitivity change (de Gouw and Warneke, 2007),

$$[XH^+] = [H_3O^+]_0 \{1 - \exp(-k\tau[X])\} \approx [H_3O^+]k\tau[X] \quad (S14)$$

where τ is the duration of the protonation process, $[H_3O^+]_0$ is the reference reagent ion signal, k is the collision rate constant, $[X]$ is the analyte mass concentration, and $[XH^+]$ is the ion signal. The approximation is valid for very small $k\tau$ values (de Gouw and Warneke, 2007). Mathematically, the approximation is valid for $\exp(-k\tau[X]) \ll 1$. Linear signal normalization and species quantification are therefore possible via the following equations,

$$[X] = \frac{1}{k\tau} \frac{[XH^+]}{[H_3O^+]} \quad (S15)$$

$$[X] = \frac{[H_3O^+]_0}{k\tau[H_3O^+]_0} \frac{[XH^+]}{[H_3O^+]} \quad (S16)$$

$$\rho_{cal} = \frac{1}{k\tau[H_3O^+]_0} \quad (S17)$$

$$[XH^+]_{norm} = \frac{[H_3O^+]_0}{[H_3O^+]} [XH^+] \quad (S18)$$

$$[X] = \rho_{cal}[XH^+]_{norm} = [X]_{ACIMS} \quad (S19)$$

where $[XH^+]_{norm}$ is the normalized gas-phase signal and is sufficient for qualitative time-series analysis. In many cases, we do not have standard compounds to obtain a calibration curve and ρ_{cal} remains unknown. The above relations break down when there is significant depletion of reagent ion, where the assumption $\exp(-k\tau[X]) \ll 1$ is no longer accurate, in which case a parallel ACIMS (P-ACIMS) formula should be applied (Wollny, 1998)

$$[X_i]_{P-ACIMS} = (k\tau)_i^{-1} \frac{X_i H^+(H_2O)_n}{\sum_j X_j H^+(H_2O)_n} \ln \left[1 + \frac{\sum_j X_j H^+(H_2O)_n}{H_3O^+(H_2O)_n} \right] \quad (S20)$$

Where $\sum_j X_j H^+(H_2O)_n^+$ is the sum of signals of products from protonation by reagent ion $H_3O^+(H_2O)_n$. For instance, the ratio of quantified concentration by ACIMS to that by P-ACIMS formula is, for n=0 (compounds such as isoprene),

$$[X_i]_{P-ACIMS} = (k\tau)_i^{-1} \frac{X_i H^+}{\sum_j X_j H^+} \ln \left[1 + \frac{\sum_j X_j H^+}{H_3O^+} \right] \quad (S21)$$

$$\frac{[X]_{ACIMS}}{[X_i]_{P-ACIMS}} = \left(\frac{[H_3O^+]}{\sum_j [X_j H^+]} \ln \left[1 + \frac{\sum_j [X_j H^+]}{[H_3O^+]} \right] \right)^{-1} \quad (S22)$$

which is a function of the reagent-to-product signal ratio, $\frac{[H_3O^+]}{\sum_j [X_j H^+]}$, hereafter referred as RPSR, as shown Fig. S2. The ACIMS correction overestimates less than 1% compared to the P-ACIMS correction for RPSR greater than 500. Overestimation greater than 5 % could be expected for RPSR < 9.8. At RPSR equal to 1, 44 % overestimation could be expected.

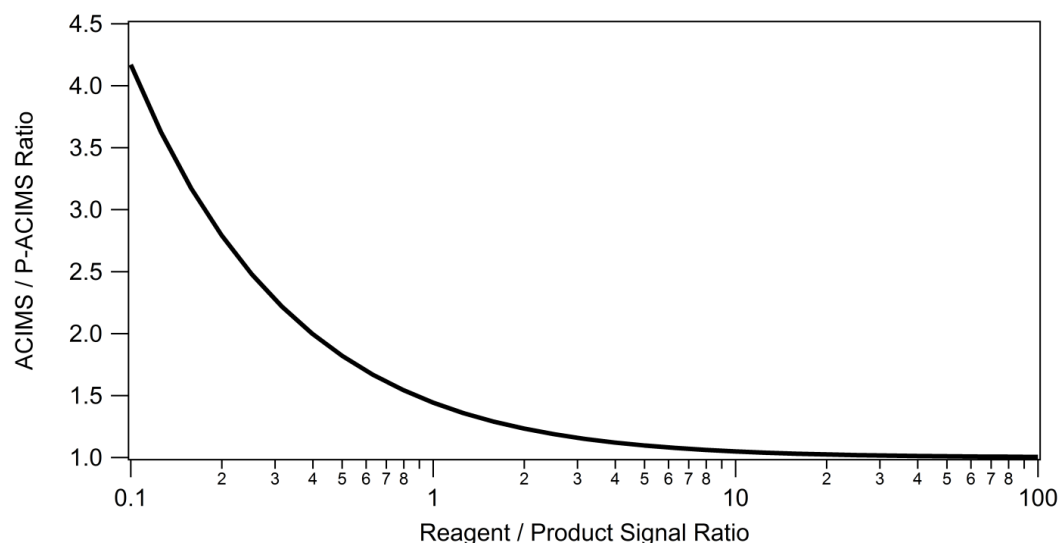


Figure S2: Estimated deviation ratio as a function of reagent-to-product signal ratio (RPSR)

S4 Particulate chlorine detection

Low levels of particulate chlorine are observed when sampling pure ammonium nitrate, ammonium sulfate, or diacid aerosols, as summarized in Table S1 and illustrated in Fig. S3a. Similar vaporizer effects/interferences have been reported for organic artifacts at m/z 44 when sampling inorganic salts (Pieber et al., 2016), which is also observed as illustrated in Fig. S3b. The interpretation of chlorine mass using the standard fragmentation table, illustrated in Table S2, relies on ions at m/z 35 and 36 and expects little interference from other ions. Observed chlorine ions when sampling pure ammonium nitrate or ammonium sulfate (Fig. S3a) were likely the result of reactions taking place at the vaporizer surface between sampled species and chlorinated residue.

10 **Table S1:** Particulate chlorine artifact signal correlations

Species	Slope ($\mu\text{g m}^{-3}/(\mu\text{g m}^{-3})$)	Intercept ($\mu\text{g m}^{-3}$)	R ²
NO ₃ (Ammo. Nitrate)	1.46×10^{-2}	-2.25×10^{-1}	0.97
SO ₄ (Ammo. Sulfate)	9.66×10^{-3}	-1.01×10^{-2}	0.80
Organics (Glutaric Acid)	6.81×10^{-3}	-4.87×10^{-2}	0.65

^aFitting parameter for particulate chlorine concentration vs. mass loading of sampled species as shown in Fig. S3a.

Table S2: Treatment of particulate chlorine in standard fragmentation table

m/z	Air ^a	Organic ^a	Chloride ^{a,b}	Cl ^{a,b}	HCl ^{a,b}
28	28				
35			frag_HCl[35],frag_Cl[35]	35, -frag_HCl[35]	0.231*frag_HCl[36]
36	0.00338*frag_air[40]		frag_HCl[36]		36, -frag_air[36]
37		37, -frag_chloride[37]	frag_HCl[37],frag_Cl[37]	0.323*frag_Cl[35]	0.323*frag_HCl[35]
38	0.000633*frag_air[40]	38, -frag_chloride[38], -frag_air[38]	frag_HCl[38]		0.323*frag_HCl[36]
40	0.01458*frag_air[28]				

^aSpecies designation used in ACSM

15 ^bAll chlorine-related signals at m/z 37 and m/z 38 are based on m/z 35 and m/z 36 measurements assuming natural isotopic abundance instead of being directly measured.

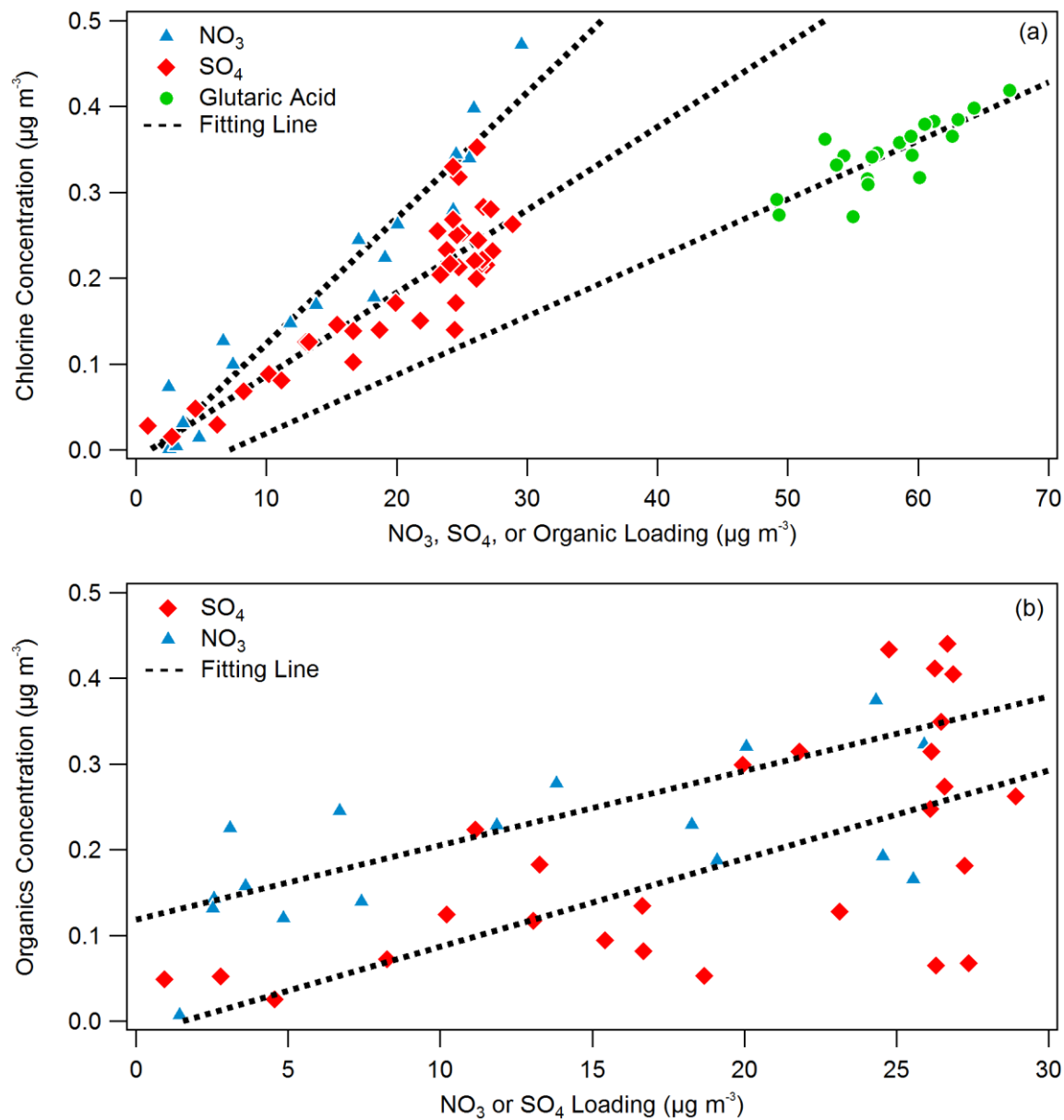


Figure S3: Observation of concentration artifact for (a) particulate chlorine when sampling lab-generated ammonium nitrate, ammonium sulfate, or pure organics aerosol, and for (b) organics when sampling lab-generated ammonium nitrate or ammonium sulfate aerosol

A particulate chlorine artifact has been observed by some Aerosol Mass Spectrometer users as well, though only ammonium nitrate appears to induce noticeable false positive chlorine signal (Jose-Luis Jimenez and Weiwei Hu, personal communications). Larger vaporizer effects might be expected in this work considering that the vaporizer effects depend on the vaporizer history (Pieber et al., 2016) and the ACSM used in this work has been exposed to elevated levels of particulate chloride. Figure S4 shows that the reported chlorine artifact concentration stems mostly from the HCl^+ (m/z 36) ion fragment.

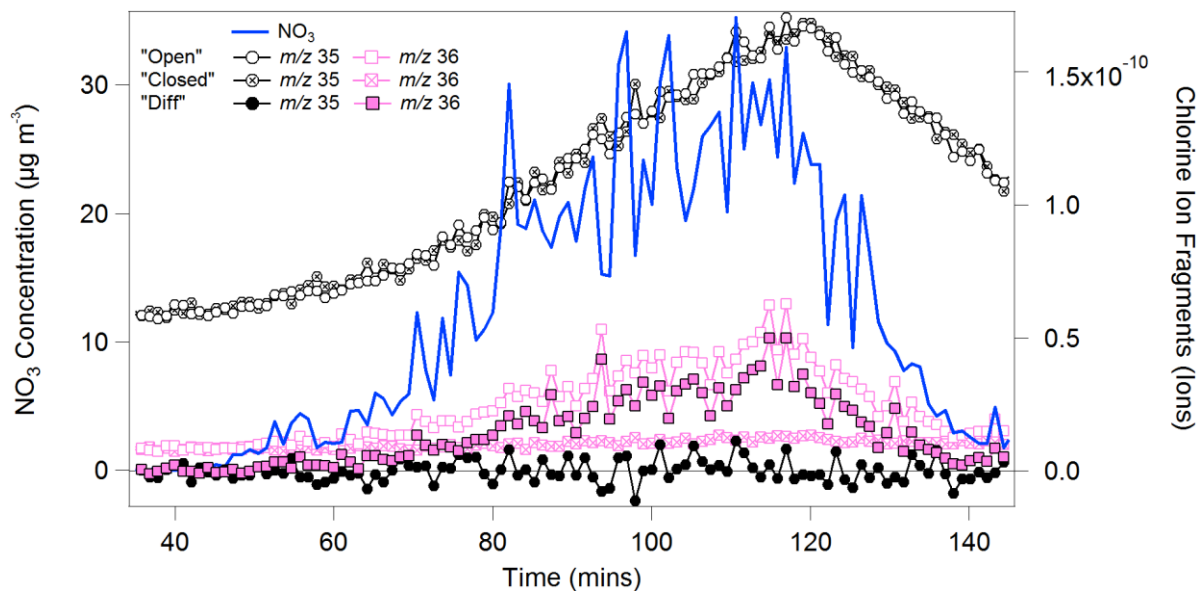


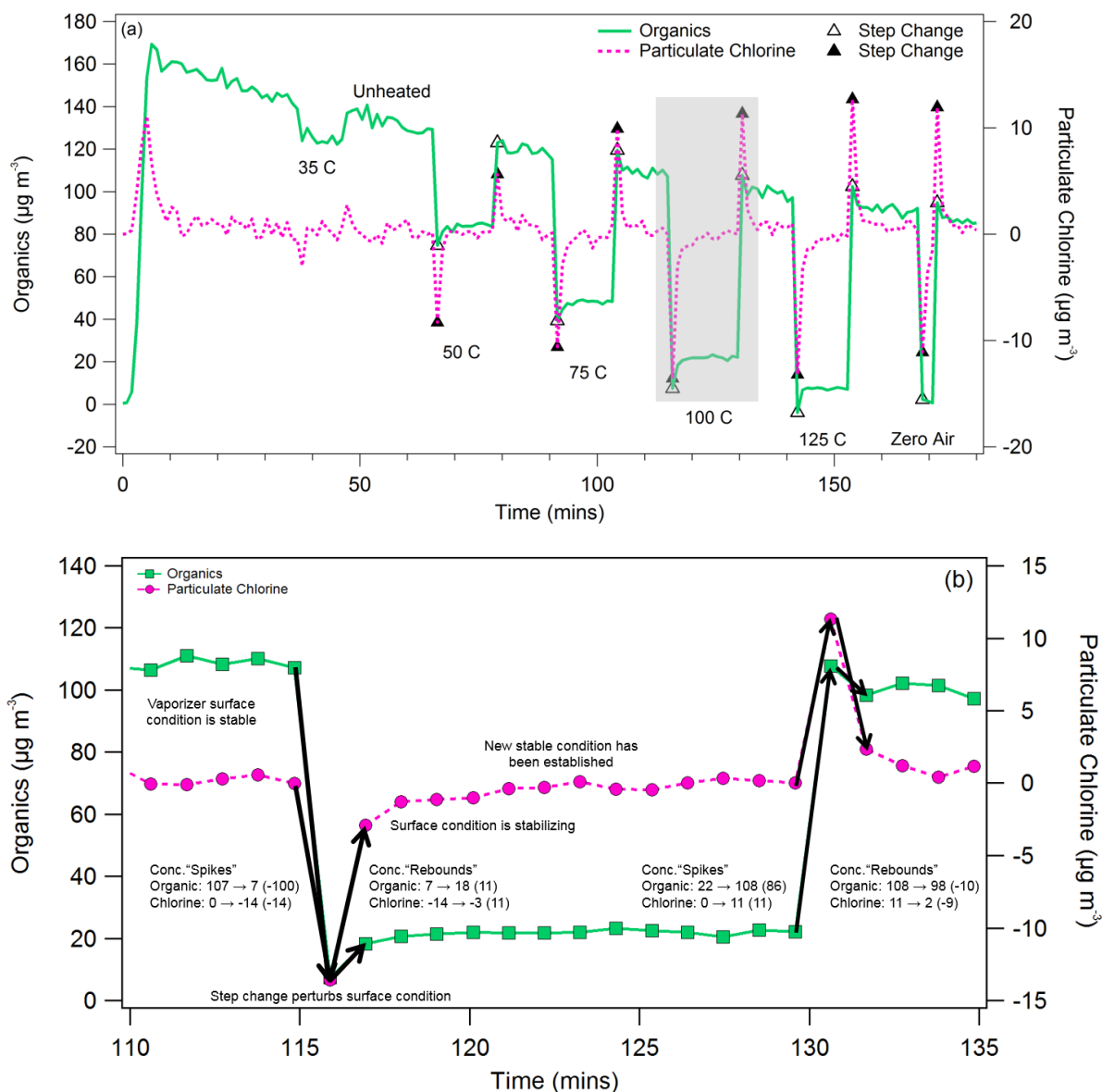
Figure S4: Ion fragments produced at m/z 35 and 36 when sampling pure ammonium nitrate. “Diff” stands for “Difference mass spectra”

This does not indicate, however, that only HCl^+ fragments are produced at the vaporizer surface. As seen in Fig. S4, m/z 35 “open” and “closed” signals also rise with increasing inorganic non-chloride salt concentrations. The apparent contribution from the m/z 35 difference mass spectra is very low because of the elevated background signals. In contrast, background signals at m/z 36 are not sensitive towards changes in non-chlorinated aerosol loading. To reduce the vaporizer chlorine artifact, long “scrubbing” sessions with inorganic salts may help remove residues from the vaporizer surface.

In the worst-case scenario, after routine exposure to particulate organochlorides, the particulate chlorine artifact is less than 1.5 % of sampled inorganic nitrate mass (Figure S3a). Because all chamber photo-oxidation experiments were conducted under low- NO_x conditions using nebulized ammonium sulfate or sulfuric acid/ammonium sulfate solutions as seeding particles, the artifact signal is expected to be well under 1 % of the total aerosol loading. Therefore, vaporizer effects alone cannot explain the high initial particulate chlorine loading (> 9 % of total SOA mass) observed in Exp. A8 (see Fig. 4).

A high concentration, initial chlorine injection experiment was carried out (Exp. S1) to further explore the ability of the ACSM to detect organochloride. Initial isoprene and chlorine concentrations were 240 and 500 ppb, respectively. The initial surface area of neutral seed aerosol was $1050 \text{ } \mu\text{m}^2 \text{ cm}^{-3}$. The UV lights were turned on for 5 minutes to form SOA and then turned off. The goal was to isolate the effect of gas-phase chemistry from particulate chlorine detection. The aerosol sample

was continuously passed through an unheated and a heated sampling tube at 1 liter per minute (LPM). As expected, lower OA concentrations were observed when sampling through the heated tube due to aerosol evaporation. Alternate sampling from unheated and heated sampling tubes introduced OA mass step changes, the magnitude of which depended on the temperature set-point (and aerosol volatility). As shown in Fig. S5a, each step change perturbed the vaporizer surface condition, resulting in a concentration “spike” until a new stable condition was achieved, as marked by the signal “rebound”, as illustrated in Fig. S5b.



10 **Figure S5:** (a) Raw particulate organics and chlorine measurement for Exp. S1. Aerosol was alternately passed through heated and unheated sampling lines; annotations show the heated line centerline temperatures. The shaded region in (a) is expanded in (b) to illustrate the definition of “spikes” and “rebounds”.

For each step decrease in aerosol concentration, the concentration “spike” (calculated as a concentration change) was negative and the concentration “rebound” (calculated as a concentration change) was positive. For each step increase in aerosol concentration, the concentration “spike” was positive and concentration “rebound” was negative. The correlation between particulate organics and chlorine “spike” and “rebound” concentrations is shown in Fig. S6.

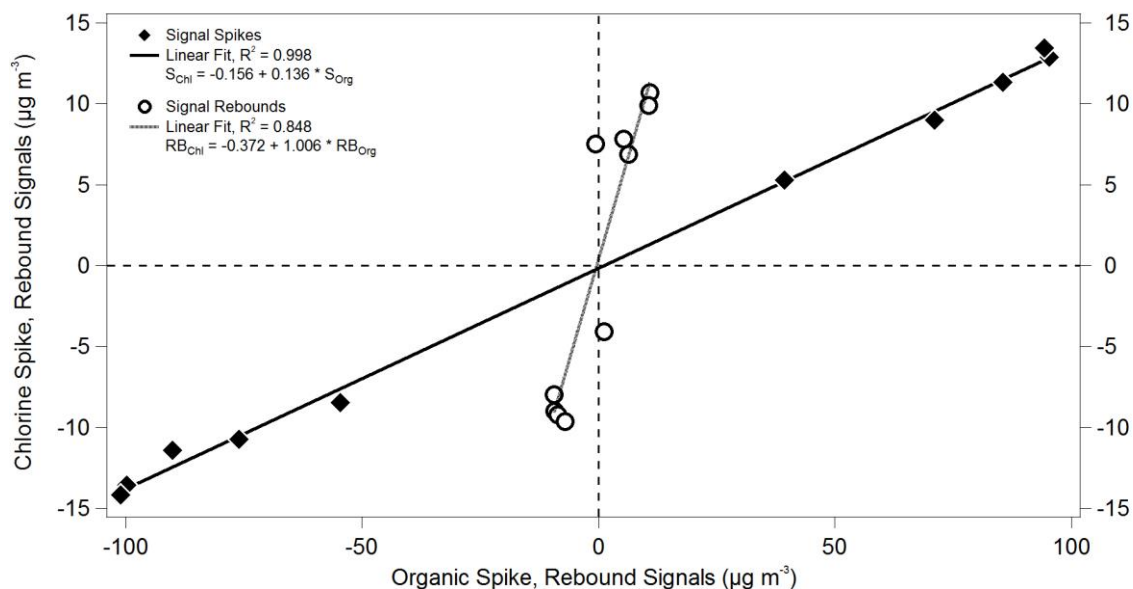
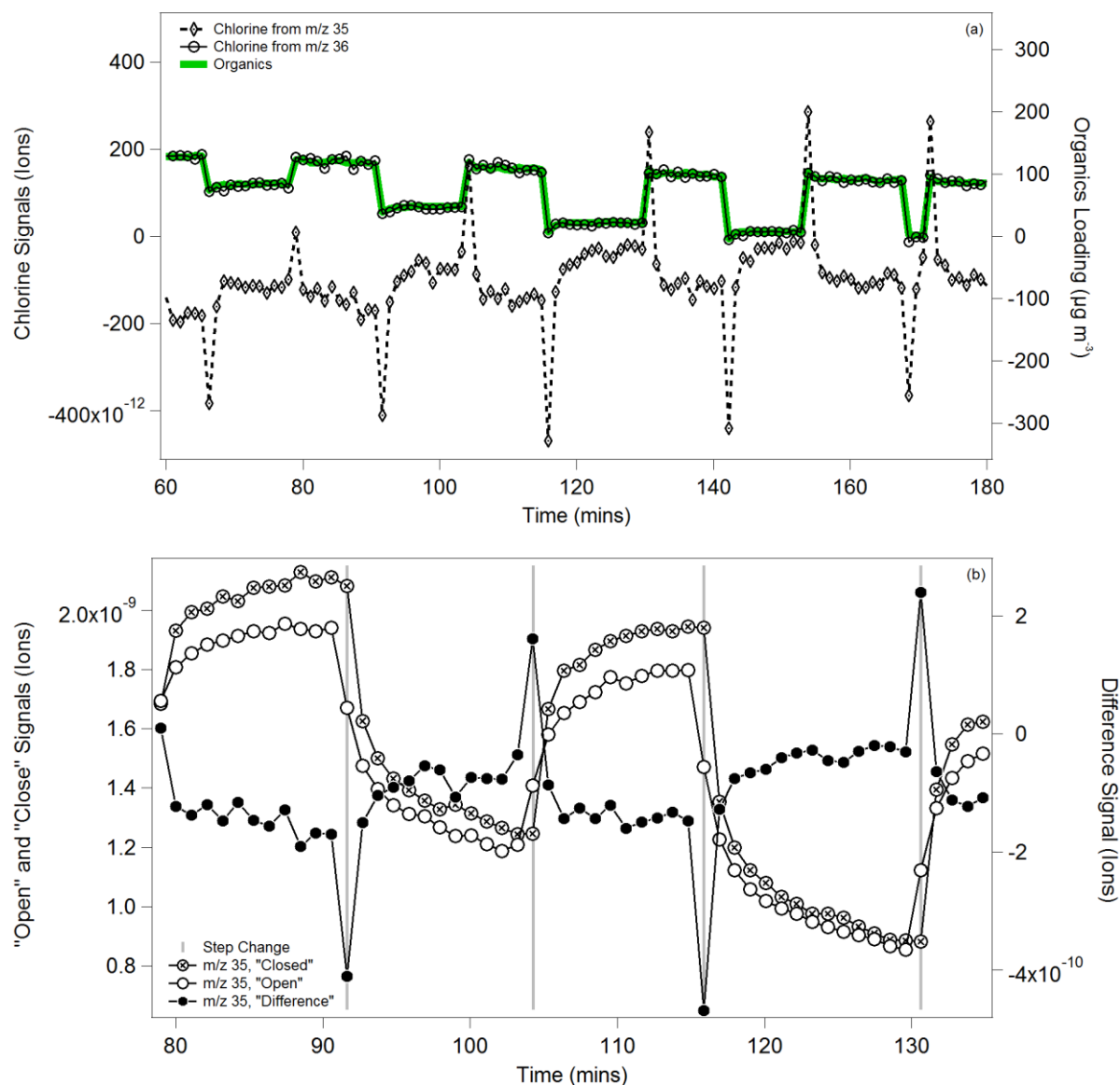


Figure S6: Organics and chlorine spikes and rebounds observed following each step change for Exp. S1. Good linear correlation between organics and chlorine was observed for both signal spikes ($R^2 \sim 0.998$) and rebounds ($R^2 \sim 0.848$).

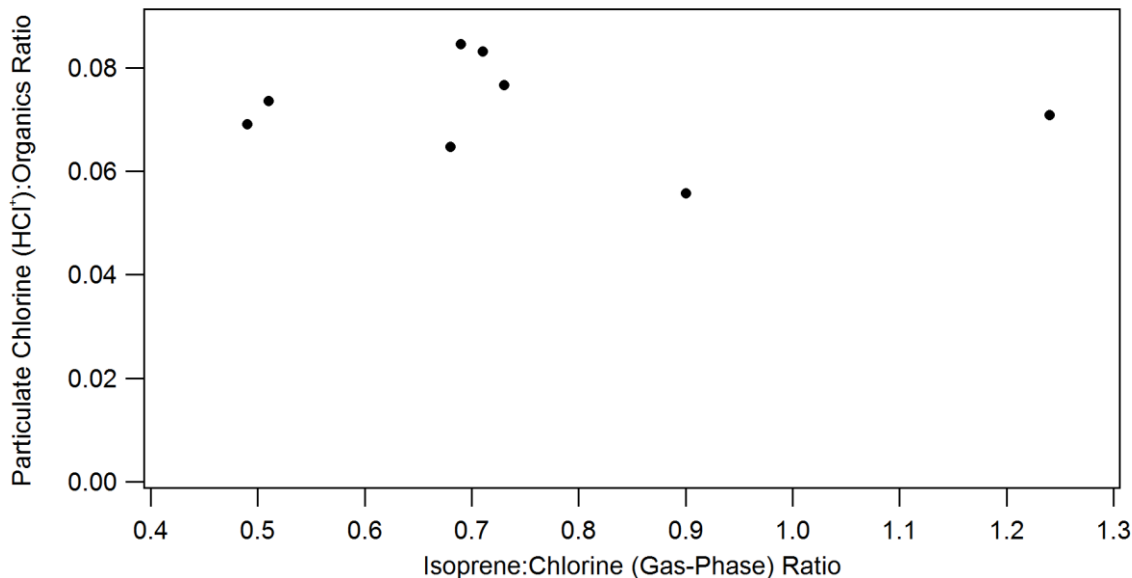
The signal “spikes” and “rebound” were likely caused by the slow vaporization (or bouncing) of particulate chlorine. Two distinct types of chlorine ions could be observed in ACSM. As shown in Fig. S7a and S7b, while the fast-desorbing chlorine (HCl^+ , m/z 36) ion fragment correlated well with OA, the slow-desorbing (Cl^+ , m/z 35) ion fragments anti-correlated with OA, where the background Cl^+ signal was consistently higher than the sample Cl^+ signal. Except for signal “spikes” and “rebounds,” the ratio of Cl^+ to HCl^+ was roughly -1:1, which is why the reported particulate chlorine concentration was near zero most of the time, even when particulate chlorine might be present. As shown in Fig. S7b, the slow-desorbing chlorine (Cl^+ , m/z 35) was responsible for the observed chlorine spikes seen in Fig. S5a. The magnitudes of the chlorine and organic spikes are shown in Fig. S6 to correlate very well ($R^2 > 0.998$) over a wide desorption (50–125 °C) and concentration (0–160 $\mu\text{g m}^{-3}$) range, indicating that organochlorides were likely present during the experiment, and that they did not differ significantly from other OA components in volatility. Good linear correlation ($R^2 > 0.848$) was also observed for the chlorine and organic signal rebounds with a slope of 1, or equal parts Cl and organics ions. The signal rebound was probably due to the build-up/removal of slow-desorbing particulate chlorine residues following each step decrease/increase in aerosol concentration. This suggests that the slow-desorbing chlorinated compounds could have undergone decomposition or oxidation on the vaporizer surface to

produce a mixture of ion fragments such as COCl^+ (56% Cl by mass), $\text{C}_2\text{H}_3\text{OCl}^+$ (45% Cl), CO_2Cl^+ (45% Cl), etc. resulting in high background chlorine signal.



- 5 **Figure S7:** (a) Fast (m/z 36)- and slow (m/z 35)-desorbing chlorine signals measured by the ACSM. Ion fragments at m/z 35 and 36 correspond to $^{35}\text{Cl}^+$ and H^{35}Cl^+ ion fragments. Contribution by $^{37}\text{Cl}^+$ and H^{37}Cl^+ (not shown) were calculated based on $^{35}\text{Cl}^+$ and H^{35}Cl^+ assuming natural isotopic abundance. The particulate chlorine “spikes” and “rebounds” shown in Fig. S5 are consistent with $^{35}\text{Cl}^+$ behavior
- 10 (b) The slow thermal desorption of chlorinated species at m/z 35 (Cl^+) leads to elevated background chlorine signals. To acquire each “difference” mass spectrum used to calculate aerosol loading, the “closed” spectrum is measured first to determine instrument background, after which the “open” spectrum is then measured. Recall that HCl^+ background is much less sensitive towards loading changes, as shown in Fig. S4.

Considering only HCl^+ ion fragments, which correlate well with OA mass, we observe the Cl-to-organics ratio to be 0.072 ± 0.01 . The ratio does not appear to correlate with isoprene concentration, gas-phase chlorine concentration, or gas-phase isoprene-to-chlorine ratio, as shown in Fig. S8.



- 5 **Figure S8:** Averaged particulate chlorine-to-organics ratio for Exp. A3–A5, A8, C2–C4, S1 plotted against gas-phase precursor isoprene-to-chlorine ratio. Particulate Cl concentration was estimated based on m/z 36 ion fragment (H^{35}Cl^+) measurement only. Exp A1, A2, and C1 were excluded from analysis due to low particulate chlorine mass concentrations. Particulate chlorine-to-organics ratio is uncorrelated with gas-phase isoprene-to-chlorine ratio ($R^2 < 0.05$), isoprene concentration (not shown, $R^2 < 0.22$), or gas-phase chlorine concentration (not shown, $R^2 < 0.08$).

S5 Effects of data selection on 1-D VBS parameter fitting

Table S3 shows parameters from VBS fits attempting to replicate a yield curve defined by complete VOC consumption where the initial VOC concentration (VOC_0) is $110 \mu\text{g m}^{-3}$, the same as the isoprene concentration used in Exp C1. Fitted VBS parameters fail to approximate the linear correlation between Y and VOC_0 .

5 **Table S3:** Fitted VBS parameters for $Y = C_{\text{OA}} / \text{VOC}_0$

C^*	10^{-4}	10^{-3}	10^{-2}	10^{-1}	10^0	10^1	10^2	10^3	10^4	10^5
10 Bins	0	0	0	0	0	0	1	1	1	1
4 Bins	0	0	0	$3.35 \cdot 10^{-3}$						
		0	0	0	$2.28 \cdot 10^{-2}$					
			0	0	0	$2.08 \cdot 10^{-1}$				
				0	0	$2.09 \cdot 10^{-2}$	1			
					0	0	1	1		
6 Bins	0	0	0	0	0	$2.08 \cdot 10^{-1}$				
		0	0	0	0	$2.09 \cdot 10^{-2}$	1			
			0	0	0	0	1	1		
				0	0	0	1	1	1	
					0	0	1	1	1	1

^aVBS fitting was performed in Matlab using the *fmincon* function. VBS parameters (α_i values) are constrained to between 0 and 1.

It is clear that 1-D VBS fitting should not and cannot be applied to yield data collected post VOC depletion. This is further illustrated in Fig. S9 for Exp. C1: VBS fittings was performed on data collected before isoprene depletion (“Pre-depletion”) and on the entire dataset (“Full”). By incorporating yield data collected post isoprene depletion, the “Full” yield curve more closely resembles the pre-defined yield curve ($Y = C_{\text{OA}} / \text{VOC}_0$). While the “pre-depletion” curve should be unique to chlorine-isoprene oxidation, the pre-defined yield curve is not.

10

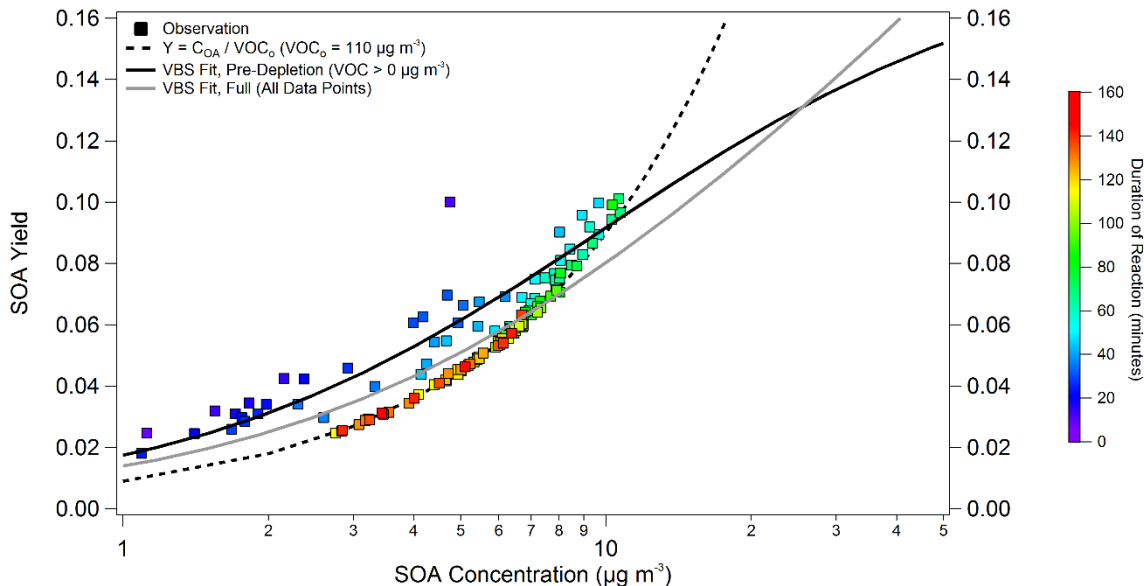


Figure S9: 1-D VBS fitting for Exp C1 with and without incorporating post depletion data.

Table S4 shows the biases introduced to the VBS results, where the “Full” fitting parameters were significantly biased towards higher volatility bins, under-predicting aerosol yield for $C_{OA} < 25 \mu\text{g m}^{-3}$ and over-predicting for $C_{OA} > 25 \mu\text{g m}^{-3}$. “Full” case fitting also overestimates the maximum yield, Y_{max} , because the “pre-defined” curve has an unlimited Y_{max} .

Table S4: Comparison of fitted VBS parameter

α_i at C^*_i	0.1	1	10	100	Y_{max}^b
Pre-Depletion ^a	4.6×10^{-4}	1.0×10^{-3}	1.8×10^{-1}	0	1.8×10^{-1}
Full	1.0×10^{-3}	0	1.2×10^{-1}	2.2×10^{-1}	3.4×10^{-1}

^a “Pre-Depletion” fitting considers only data acquired prior to the complete consumption of isoprene; “Full” fitting encompasses measurements acquired after isoprene depletion.

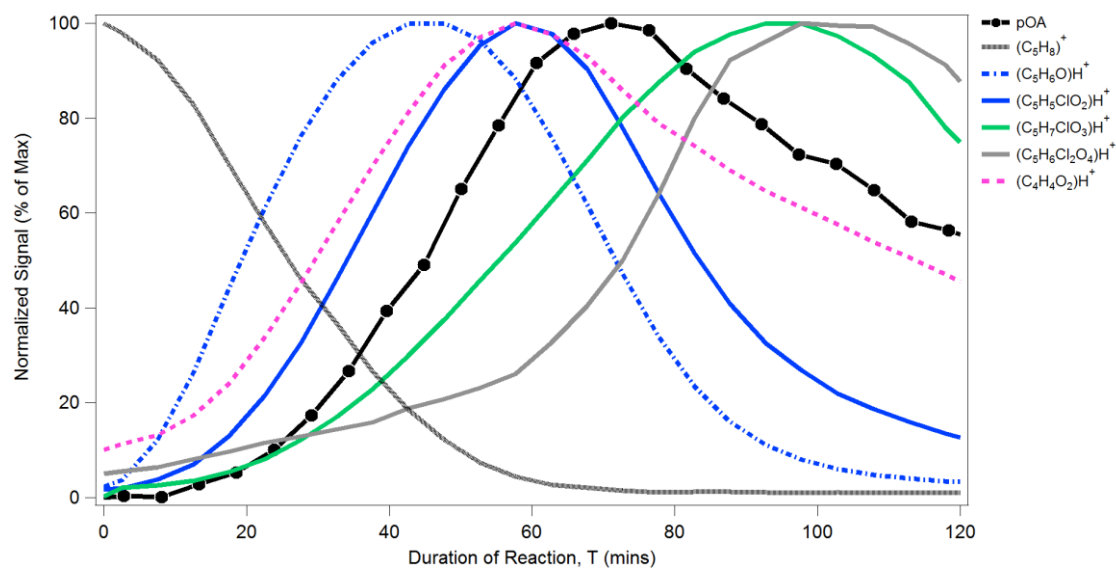
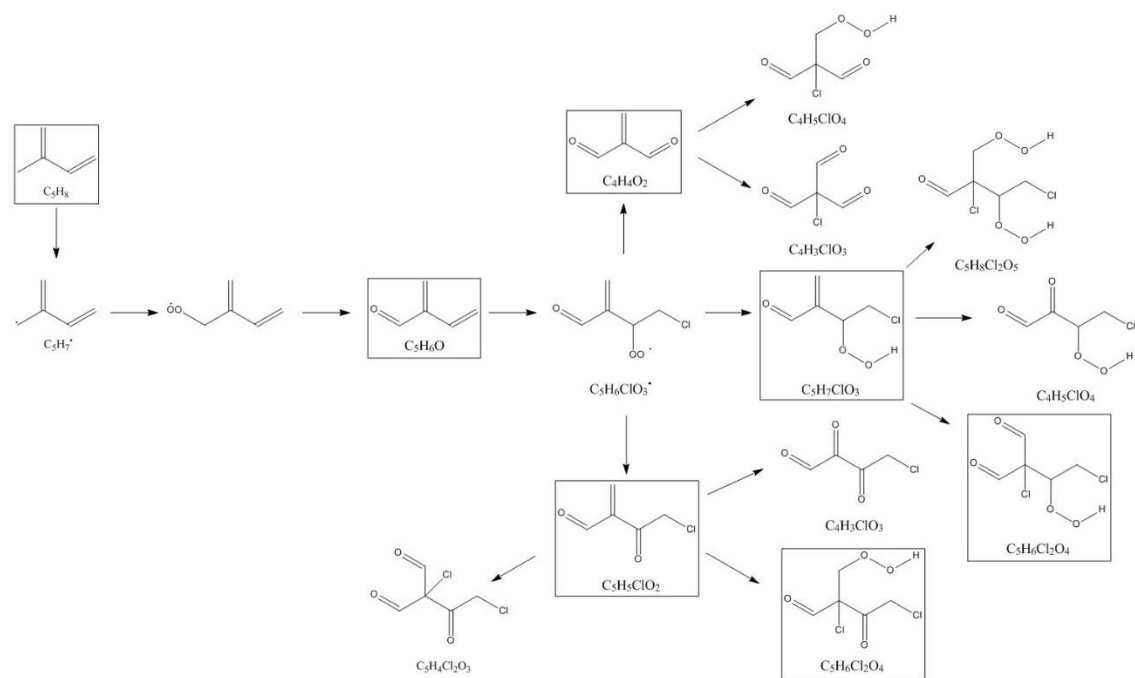
^b Maximum SOA yield, see Eq. (10)

S6. Multi-generational chemistry and proposed reaction pathways

Potential reaction pathways and observation of ions consistent with proposed reaction products are shown for select compounds, including C_5H_6O in Fig. S10, C_5H_9ClO in Fig. S11, and C_5H_8O in Fig. S12. Products observed using CIMS are framed in the reaction pathway graphs. Only one isomeric configuration is shown per chemical formula. Products that are

5 not observed by CIMS may have low sensitivity, may exist primarily in the particle-phase, or may have not been formed.

Below, C_5H_6O is a H-abstraction pathway product containing two double bonds which could undergo chlorine addition reactions, as shown in Fig. S10a.



5

Figure S10. (a, top) Proposed reaction pathways for C_5H_6O oxidation products, and (b, bottom) time-series of products observed in $(H_2O)_nH_3O^+$ CIMS.

Below, $C_5H_9ClO_2$ is a Cl-addition reaction pathway product produced when the RO_2 radical undergoes the $RO_2 + HO_2$ reaction pathway as opposed to the $RO_2 + RO_2$ reaction pathway. Because HO_2 radicals are produced from $RO_2 + RO_2$ reactions, $C_5H_9ClO_2$ formation is delayed compared to C_5H_7ClO , which is shown to form very early on during the photo-oxidation process in Fig. 6a in the main text. Continued oxidation by chlorine radical is possible, as shown in Fig. S11a.

5

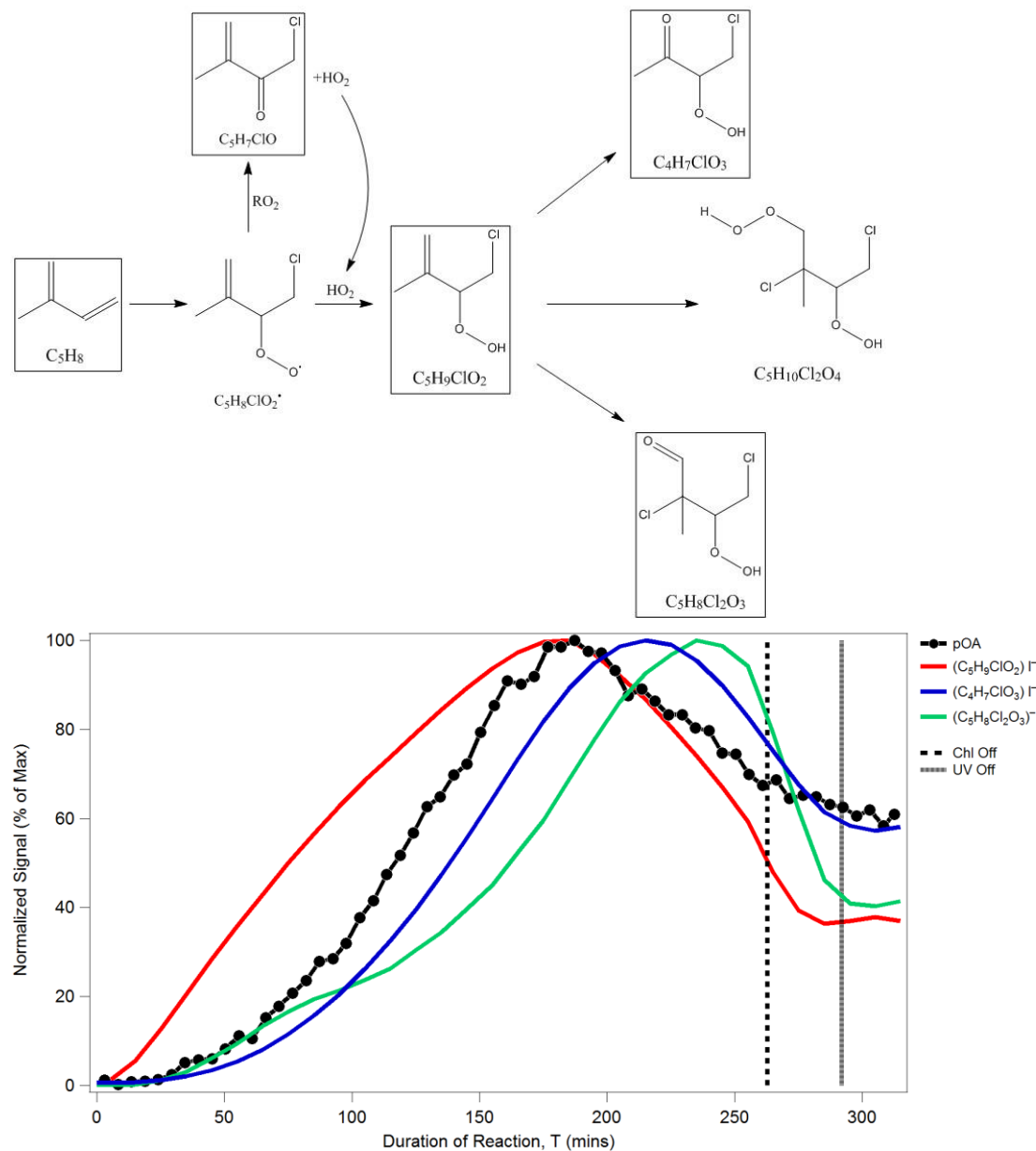
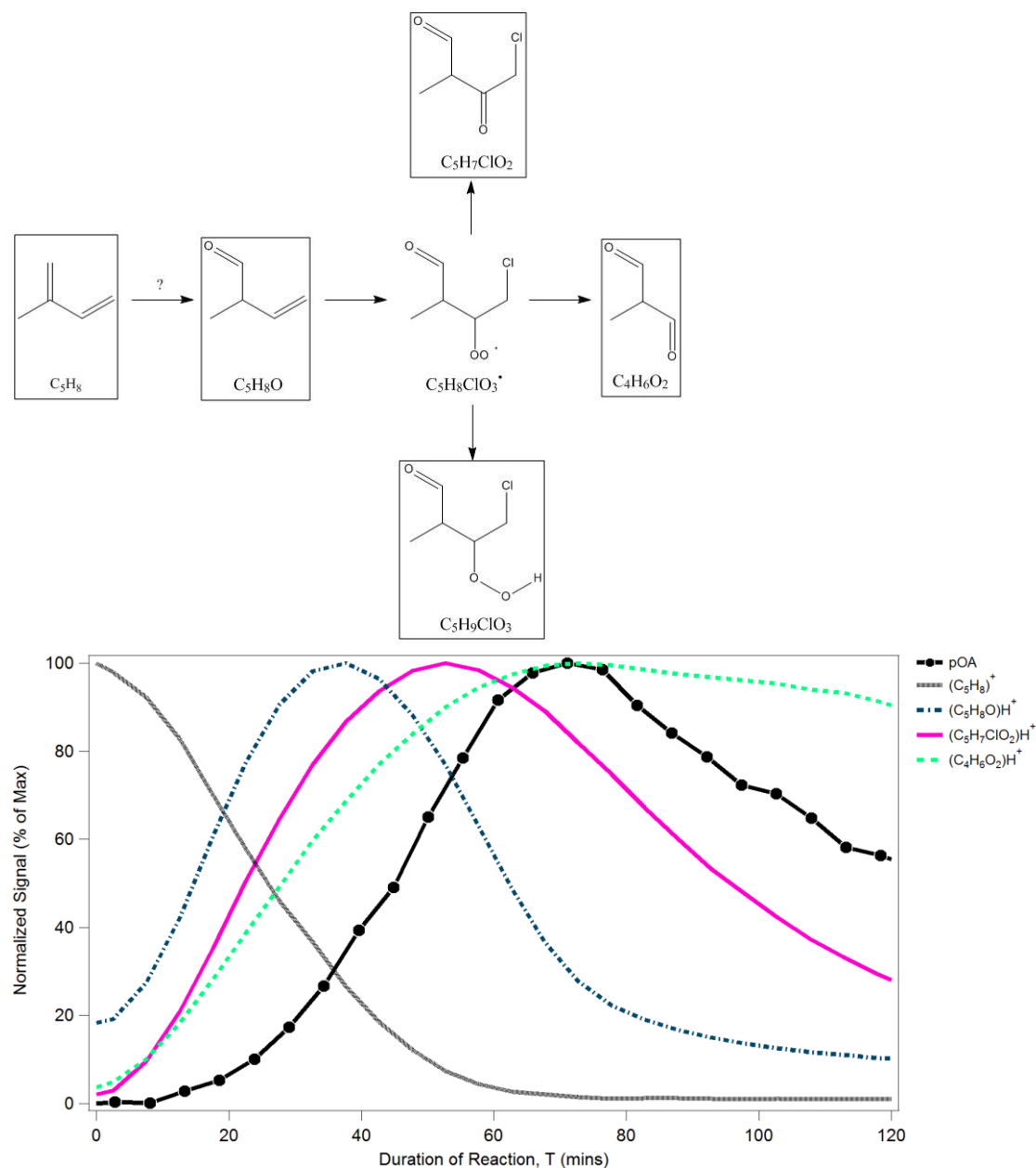


Figure S11. (a, top) Proposed reaction pathways for $C_5H_9ClO_2$ and its oxidation products, and (b, bottom) time-series of products observed in $(H_2O)_nI^-$ CIMS. C_5H_7ClO is observed using $(H_2O)_nH_3O^+$ CIMS (see Fig.6a).

Below, C_5H_8O is possibly an OH-isoprene oxidation product. As discussed in the main text, the formation mechanism for C_5H_8O is unclear. Continued oxidation by chlorine-radical is possible, as shown in Fig. S12. Reaction product $C_5H_9ClO_3$ is observed in iodide-water CIMS.

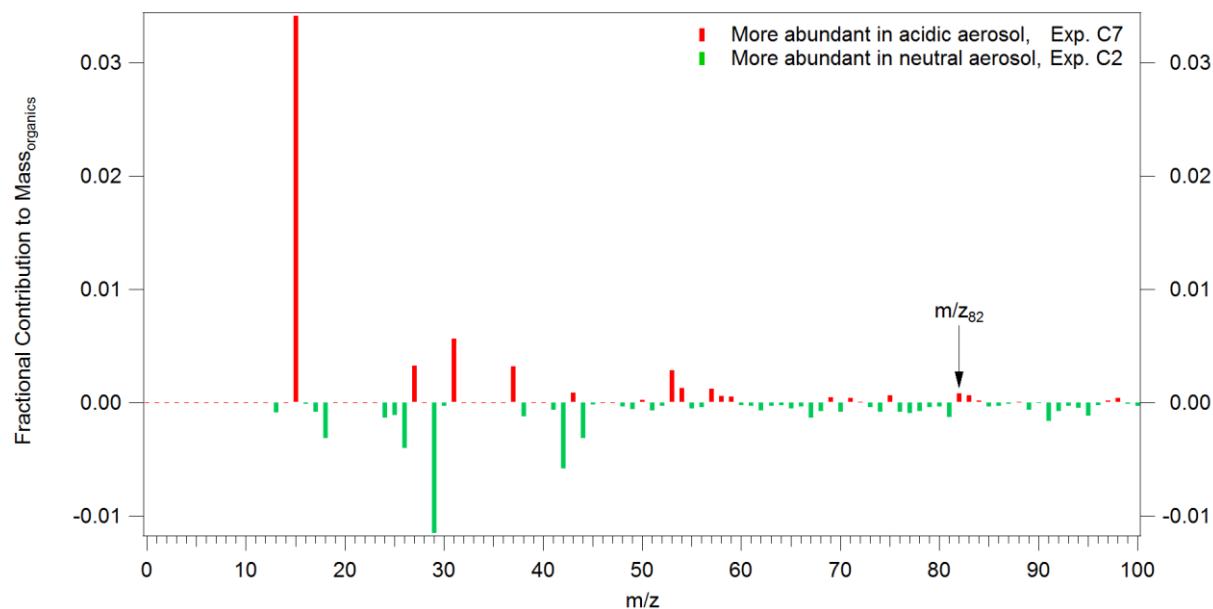


5

Figure S12. (a) Proposed reaction pathways for C_5H_8O oxidation products, and (b, bottom) corresponding time-series observed in $(H_2O)_nH_3O^+$ CIMS. Reaction product $C_5H_9ClO_3$ was observed in $(H_2O)_nI^-$ CIMS (see Fig. 6b).

S7. Effect of aerosol acidity

Contribution to overall organic aerosol mass from ion fragments at m/z 82 ($C_5H_6O^+$ and potentially other interfering ions), f_{82} increases from 5.5 ‰ to 6.4‰ in the presence of acidic aerosol, as shown in Fig S13 below. Although this behavior is consistent with enhanced uptake of IEPOX onto acidic aerosols (Budisulistiorini et al., 2013; Gaston et al., 2014; Hu et al., 2015; Lin et al., 2012; Riedel et al., 2015, 2016), the f_{82} value observed using neutral seed (5.5 ‰) is only slightly above the f_{82} values determined in CI-monoterpene oxidation experiments using the same ACSM (5 ‰). Therefore, our data does not provide evidence for a significant contribution of IEPOX to SOA formation.



10 **Figure S13.** Comparison of ACSM unit mass spectra. Red bars indicate m/z fragments enhanced in the presence of acidic aerosols. Green bars indicate m/z fragments enhanced in the presence of neutral aerosols.

Figure S14 shows the effects of acidic aerosol on gas-phase species observed by $(\text{H}_2\text{O})_n\text{H}_3\text{O}^+$ and $(\text{H}_2\text{O})_n\text{I}^-$ CIMS. Unit mass spectra over the first 120 minutes of photooxidation from neutral seed (C3, C5) and acidic seed experiments (C6 and C7) were averaged and compared. Due to differences in precursor concentrations used, signals are normalized to the most abundant gas-phase species observed, which were $(\text{C}_5\text{H}_6\text{O}_2)^+$ at m/z 99 in positive mode and $(\text{Cl}_2)\text{I}^-$ at m/z 197 in negative mode. Presence of acidic aerosol appears to lead to uniform decreases in gas-phase species concentrations. Formation of $\text{C}_5\text{H}_6\text{O}_2$ from isoprene-Cl reactions has been proposed previously (Nordmeyer et al., 1997), but the pathway is unknown.

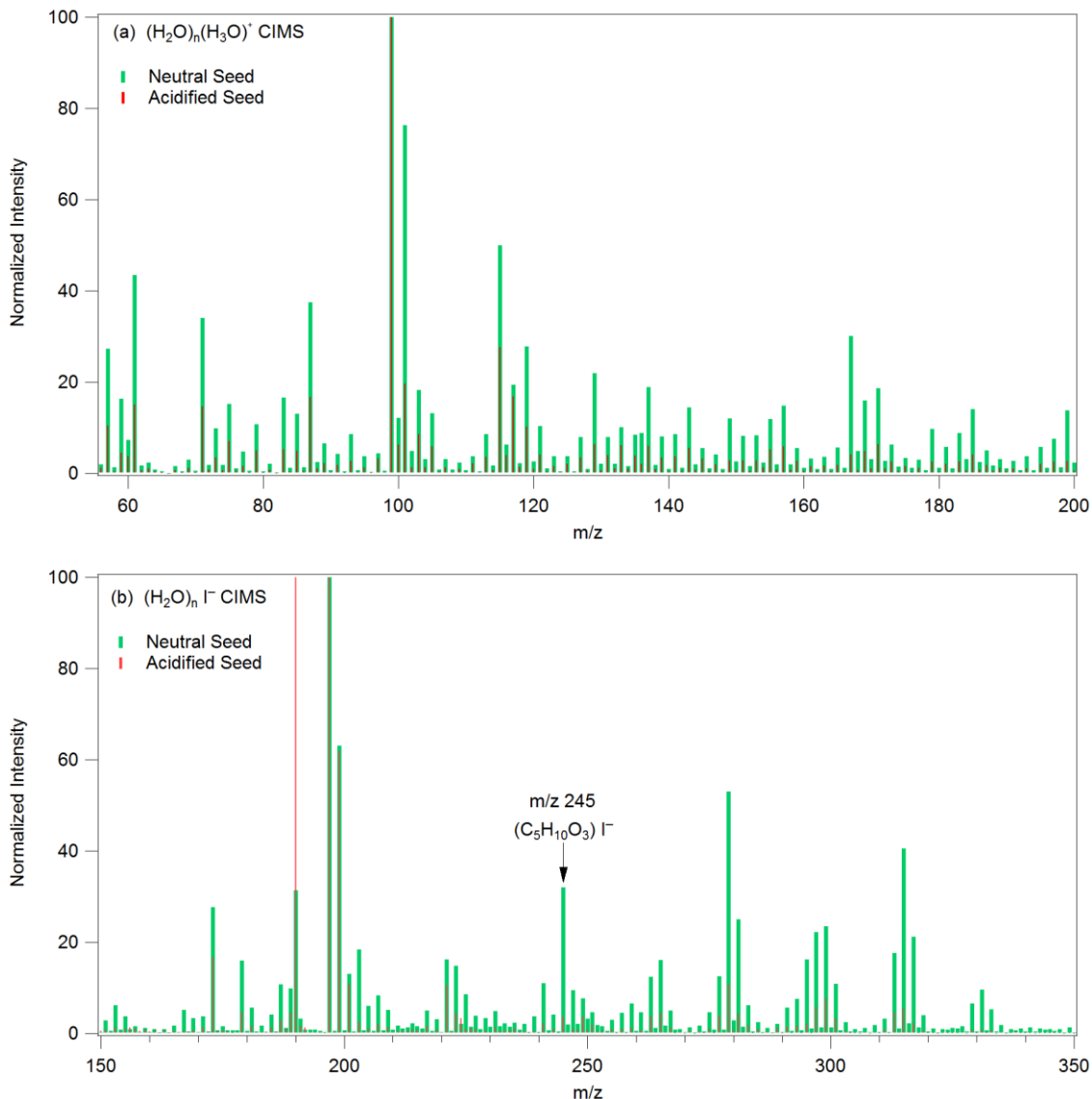


Figure S14. Unit mass spectra (UMR) of (a) positive mode measurement, where UMR ion intensities are normalized against the most intense photo-oxidation product ion signal at m/z 99, and of (b) negative mode measurement, where the ion intensities are normalized against chlorine-iodide adduct at m/z 197. The representative spectra are from experiment C3 ($[\text{H}_2\text{O}]_n\text{I}^-$ /neutral seed), C5 ($[\text{H}_2\text{O}]_n\text{H}_3\text{O}^+$ /neutral seed), C6 ($[\text{H}_2\text{O}]_n\text{I}^-$ /acidic seed), and C7 ($[\text{H}_2\text{O}]_n\text{H}_3\text{O}^+$ /acidic seed).

References

- Budisulistiorini, S. H., Canagaratna, M. R., Croteau, P. L., Marth, W. J., Baumann, K., Edgerton, E. S., Shaw, S. L., Knipping, E. M., Worsnop, D. R., Jayne, J. T., Gold, A. and Surratt, J. D.: Real-time continuous characterization of secondary organic aerosol derived from isoprene epoxydiols in downtown Atlanta, Georgia, using the aerodyne aerosol chemical speciation monitor, *Environ. Sci. Technol.*, 47(11), 5686–5694, doi:10.1021/es400023n, 2013.
- Canagaratna, M. R., Jimenez, J. L., Kroll, J. H., Chen, Q., Kessler, S. H., Massoli, P., Hildebrandt Ruiz, L., Fortner, E., Williams, L. R., Wilson, K. R., Surratt, J. D., Donahue, N. M., Jayne, J. T. and Worsnop, D. R.: Elemental ratio measurements of organic compounds using aerosol mass spectrometry: Characterization, improved calibration, and implications, *Atmos. Chem. Phys.*, 15(1), 253–272, doi:10.5194/acp-15-253-2015, 2015.
- 10 Donahue, N. M., Robinson, A. L., Stanier, C. O. and Pandis, S. N.: Coupled partitioning, dilution, and chemical aging of semivolatile organics, *Environ. Sci. Technol.*, 40(8), 2635–2643, doi:10.1021/es052297c, 2006.
- Donahue, N. M., Kroll, J. H., Pandis, S. N. and Robinson, A. L.: A two-dimensional volatility basis set-Part 2: Diagnostics of organic-aerosol evolution, *Atmos. Chem. Phys.*, 12(2), 615–634, doi:10.5194/acp-12-615-2012, 2012.
- Gaston, C. J., Riedel, T. P., Zhang, Z., Gold, A., Surratt, J. D. and Thornton, J. A.: Reactive uptake of an isoprene-derived epoxydiol to submicron aerosol particles, *Environ. Sci. Technol.*, 48(19), 11178–11186, doi:10.1021/es5034266, 2014.
- 15 de Gouw, J. and Warneke, C.: Measurements of volatile organic compounds in the earth's atmosphere using proton-transfer-reaction mass spectrometry, *Mass Spectrom. Rev.*, 26(2), 223–257, doi:10.1002/mas.20119, 2007.
- Heald, C. L., Kroll, J. H., Jimenez, J. L., Docherty, K. S., Decarlo, P. F., Aiken, A. C., Chen, Q., Martin, S. T., Farmer, D. K. and Artaxo, P.: A simplified description of the evolution of organic aerosol composition in the atmosphere, *Geophys. Res. Lett.*, 37(8), doi:10.1029/2010GL042737, 2010.
- 20 Hu, W. W., Campuzano-Jost, P., Palm, B. B., Day, D. A., Ortega, A. M., Hayes, P. L., Krechmer, J. E., Chen, Q., Kuwata, M., Liu, Y. J., De Sá, S. S., McKinney, K., Martin, S. T., Hu, M., Budisulistiorini, S. H., Riva, M., Surratt, J. D., St. Clair, J. M., Isaacman-Van Wertz, G., Yee, L. D., Goldstein, A. H., Carbone, S., Brito, J., Artaxo, P., De Gouw, J. A., Koss, A., Wisthaler, A., Mikoviny, T., Karl, T., Kaser, L., Jud, W., Hansel, A., Docherty, K. S., Alexander, M. L., Robinson, N. H.,
- 25 Coe, H., Allan, J. D., Canagaratna, M. R., Paulot, F. and Jimenez, J. L.: Characterization of a real-time tracer for isoprene epoxydiols-derived secondary organic aerosol (IEPOX-SOA) from aerosol mass spectrometer measurements, *Atmos. Chem. Phys.*, 15(20), 11807–11833, doi:10.5194/acp-15-11807-2015, 2015.
- Kroll, J. H., Donahue, N. M., Jimenez, J. L., Kessler, S. H., Canagaratna, M. R., Wilson, K. R., Altieri, K. E., Mazzoleni, L. R., Wozniak, A. S., Bluhm, H., Mysak, E. R., Smith, J. D., Kolb, C. E. and Worsnop, D. R.: Carbon oxidation state as a metric for describing the chemistry of atmospheric organic aerosol., *Nat. Chem.*, 3(2), 133–139, doi:10.1038/nchem.948, 2011.
- 30

- Lin, Y. H., Zhang, Z., Docherty, K. S., Zhang, H., Budisulistiorini, S. H., Rubitschun, C. L., Shaw, S. L., Knipping, E. M., Edgerton, E. S., Kleindienst, T. E., Gold, A. and Surratt, J. D.: Isoprene epoxydiols as precursors to secondary organic aerosol formation: Acid-catalyzed reactive uptake studies with authentic compounds, *Environ. Sci. Technol.*, 46(1), 250–258, doi:10.1021/es202554c, 2012.
- 5 Nordmeyer, T., Wang, W., Ragains, M. L., Finlayson-Pitts, B. J., Spicer, C. W. and Plastridge, R. A.: Unique products of the reaction of isoprene with atomic chlorine: Potential markers of chlorine atom chemistry, *Geophys. Res. Lett.*, 24(13), 1615–1618, doi:10.1029/97GL01547, 1997.
- Pieber, S. M., El Haddad, I., Slowik, J. G., Canagaratna, M. R., Jayne, J. T., Platt, S. M., Bozzetti, C., Daellenbach, K. R., Fröhlich, R., Vlachou, A., Klein, F., Dommen, J., Miljevic, B., Jiménez, J. L., Worsnop, D. R., Baltensperger, U. and
10 Prévôt, A. S. H.: Inorganic salt interference on CO₂⁺ in Aerodyne AMS and ACSM organic aerosol composition studies, *Environ. Sci. Technol.*, 50(19), 10494–10503, doi:10.1021/acs.est.6b01035, 2016.
- Riedel, T. P., Lin, Y. H., Budisulistiorini, S. H., Gaston, C. J., Thornton, J. A., Zhang, Z., Vizuete, W., Gold, A. and Surratt, J. D.: Heterogeneous reactions of isoprene-derived epoxides: Reaction probabilities and molar secondary organic aerosol yield estimates, *Environ. Sci. Technol. Lett.*, 2(2), 38–42, doi:10.1021/ez500406f, 2015.
- 15 Riedel, T. P., Lin, Y. H., Zhang, Z., Chu, K., Thornton, J. A., Vizuete, W., Gold, A. and Surratt, J. D.: Constraining condensed-phase formation kinetics of secondary organic aerosol components from isoprene epoxydiols, *Atmos. Chem. Phys.*, 16(3), 1245–1254, doi:10.5194/acp-16-1245-2016, 2016.
- Sellegrì, K., Umann, B., Hanke, M. and Arnold, F.: Deployment of a ground-based CIMS apparatus for the detection of organic gases in the boreal forest during the QUEST campaign, *Atmos. Chem. Phys.*, 5(2), 357–372, doi:10.5194/acp-5-357-2005,
20 2005.
- Wollny, A.G.: Flugzeugmessungen atmosphärischer Spurengase mittels Ionen-Molekül-Reaktions-Massenspektrometrie, 1998. Retrieved with permission from University Library Heidelberg BPA. SWB-PPN: 074540750